Synthesis and performance optimisation of spray coated Cu_2ZnSnS_4 absorbing layers from single-source xanthate precursors

M. T. Bishop[a,b], L. Zhang[b], A. Dolganov[b], G. Z. Chen[b,c], C. Peng[b,d,**], D. Hu[b,e,*]

[a] *International Doctoral Innovation Centre, University of Nottingham Ningbo China, Ningbo, 315100, PR China*
[b] *Department of Chemical and Environmental Engineering, Faculty of Science and Engineering, University of Nottingham Ningbo China, 315100, PR China*
[c] *Department of Chemical and Environmental Engineering, Advanced Materials Research Group, Faculty of Engineering, University of Nottingham, Nottingham NG7 2RD, UK*
[d] *Wuhan University, School of Resource and Environmental Science, Wuhan 30079, Hubei, PR China*
[e] *Advanced Energy and Environmental Materials & Technologies Research Group, The University of Nottingham Ningbo China, Ningbo 315100, PR China*

Abstract

Cu_2ZnSnS_4 (CZTS) is a promising non-toxic and cheap absorber layer for the use in photovoltaic cells. In this work copper, zinc and tin xanthates were synthesised and deposited using a single-source spray coating technique to produce CZTS thin films, to investigate how the ratio of these precursors can alter the performance of the device. It was determined that using a tin rich xanthate precursor mix resulted in the thin film with the chemical composition closest to CZTS, with few contaminating phases (i.e. $Cu_{2-x}S$, Cu_2SnS_3 and ZnS). To explain this observation, isothermal thermal gravimetric analysis was used to determine rate constants for the decomposition of these xanthate precursors. The rate constants of copper xanthate and zinc xanthate align very well (1.26 and 1.24 s^{-1} respectively). However, the rate constant for tin xanthate differs significantly (1.09 s^{-1}). Therefore, to form the appropriate ratio in the final product, a tin rich precursor mixture is required. This tin rich xanthate sample was shown to have a band gap of

*di.hu@nottingham.edu.cn
**chuang.peng@whu.edu.cn

1.73 eV and a power conversion efficiency of 0.15 %.

Keywords: Copper zinc tin sulfide; Xanthate; Spray deposition; Thin Film Solar Cells

1. Introduction

CZTS solar cells refer to a thin film of Cu_2ZnSnS_4, a semiconducting material consisting of only abundant, cheap and non-toxic materials, and a band gap of roughly 1.5 eV [1–7]. Solar cells utlising CZTS absorber layers have been shown to display Power Conversion Efficiencies (PCEs) exceeding 10 %, and are predicted to continually rise [3, 6]. Therefore, CZTS based solar cells have attracted much interest in recent years.

In an effort to try and prepare these devices, many different deposition methods have been investigated to optimise the performance of CZTS films, including electrochemical deposition [8–10], magnetron sputtering [5, 11–15], inkjet printing [16], spray pyrolysis [17, 18], and spin coating [3]. However, these prevalent methods deposit CZTS as a two-step process, requiring additional sulfurisation steps [10, 14, 15, 17–20]. Using a two-step method adds additional costs and scale-up issues when looking for the future industrialisation of the technique. On the other hand, by developing a single-step deposition technique that could effectively deposit CZTS, the future industrialisation of this technique could be greatly enhanced. It has been reported that spray coating is an effective single-step deposition technique [21]. Due to the inherent simplicity of this technique, high speed fabrication of devices is possible for laboratory applications, while also allowing for easy scale-up to commercialisation [21]. Though, this would require the use of an appropriate single-source precursor, to enable to deposition of a metal sulfide without the need for an additional sulfur source.

Therefore, it is highly beneficial to select an appropriate precursor for the single-step deposition of CZTS active layers, while also utilising a highly scalable process. Furthermore, the selected precursor should preferably function as a low temperature precursor, as it has been well reported that high temperatures can result in the loss volatile components (such as SnS and S) damaging the stoichiometry of the CZTS active layer [18, 20, 22–24].

Metal xanthates have been used as a low temperature single-source precursor to form metal sulfides, with the general formula $[M(S_2COR)_n]$, where R is an alkyl group, and have been shown to be viable precursors for Cu_2ZnSnS_4

[21, 25–29]. It has been suggested that metal xanthates decompose via the Chugaev elimination reaction [30], as shown in **Figure 1**.

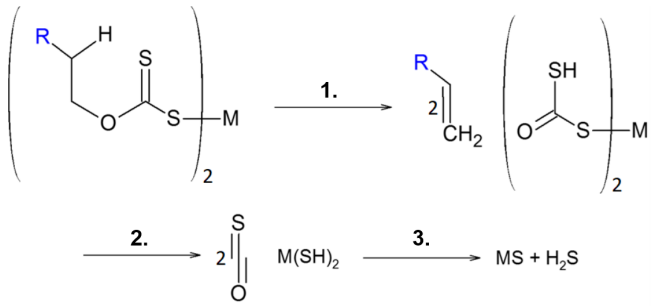

Figure 1: General reaction mechanism for Chugaev elimination reaction.

This reaction mechanism consists of three steps:

1. *A syn-elimination of an alkene via a 6-membered cyclic transition state.*
2. *Carbonyl sulfide elimination.*
3. *A hydrogen sulfide elimination process.*

By combining metal xanthate precursors with spray coating, a smooth transition from the laboratory scale to an industrial scale can be easily facilitated [1], as metal xanthates allow for the straightforward deposition of metal sulfide thin films, without the need of an additional expensive or time consuming method.

Fischereder et al. first presented the synthesis and characterization of these new metal xanthate precursors and the preparation of CZTS films, using Cu(^{i}HexXan), Zn(^{i}HexXan)$_2$, and [SnS$_2$(^{i}HexXan)$_2$]; where (^{i}HexXan) refers to $S_2COCH(CH_3)C(CH_3)_3$ [3]. Despite the CZTS films being stoichiometrically accurate, exhibiting a very high absorption coefficient (>2x10^5 cm^{-1}) and a band gap of 1.31 eV, the reported efficiencies were roughly 0.1 % [3]. Since this, other xanthate precursors for depositing CZTS have been synthesised and demonstrated, however, no attempt has been made to improve their power conversion efficiency [1, 28], leaving a large scope for the investigation into depositing CZTS solar cells via xanthate precursors, addressing key areas and aspects for improving this highly commercial approach.

Furthermore, despite the successful demonstration of CZTS deposition via xanthate precursors, many difficulties remain in controlling this deposition [1, 3, 28]. These challenges are related to matching the temperature window for decomposition and the kinetics of these decomposition processes [28].

Therefore it is of great significance to address how the chemical composition of the precursor mix alters the device.

This work focuses on the synthesis and spray coating of four metal xanthate precursors (Cadmium Ethyl Xanthate, Copper (I) Ethyl Xanthate, Zinc Ethyl Xanthate and Tin (IV) Ethyl Xanthate). These samples were deposited using spray coating, a previously utilised technique with high versatility and low cost [7, 31, 32]. The chemical composition of the single-source precursor was altered to investigate how this impacts the performance of deposited devices. Isothermal Thermal Gravimetric Analysis (TGA) was conducted in order to determine the rate constants for decomposition for the metal xanthate precursors, allowing for key issues and results to be highlighted for fabricating a CZTS based solar cell using a single–source precursor process.

2. Methodology

2.1. Metal Xanthate Synthesis

Each procedure of xanthate synthesis followed a similar synthetic route proposed by Agrawal el al [33].

2.1.1. Cadmium Ethyl Xanthate (CdXan) synthesis

3.5 g of potassium ethyl xanthate dissolved in 20 ml of de-ionized water and added drop wise to 1 g of cadmium chloride dissolved in 20 ml of de-ionized water. This aqueous solution was then stirred for 24 hours, revealing a pale yellow precipitate. Finally, the prepared precipitate was filtered, washed with de-ionized water and dried at 50 °C.

^{1}H NMR (300 MHz, $CDCl_3$): $\delta = 4.43$ (q, 4H), 1.32 (t , 6H) ppm.

Calc. for $C_6H_{10}O_2S_4Cd$ (%): C 20.3, S 36.1, Cd 31.7; found: C 20.0, S 36.2, Cd 32.2.

2.1.2. Copper (I) Ethyl Xanthate (CuXan) synthesis

Copper(II) chloride dihydrate (0.9 g) was dissolved in 20 ml of de-ionized water. Then, an aqueous solution of potassium ethyl xanthate (3.5 g dissolved in 20 ml of de-ionized water) was gradually added drop wise to the copper dichloride solution under gentle stirring. The reaction was allowed to stir for 24 hours. The orange precipitate was filtered off, washed in ethanol and dried under vacuum to obtain CuXan as a yellow powder. It is important to note that, despite the use of copper (II) chloride as a reagent in the synthesis of CuXan, the product is noted to be copper (I) xanthate. This is

a well-established phenomena and is attributed to the reduction of the formed copper (II) xanthate to copper (I) xanthate via a self-redox reaction, with metal-free xanthate dimers ($(S_2COR)_2$) remaining as a byproduct [3, 34].

^{1}H NMR (300 MHz, $CDCl_3$): $\delta = 4.69$ (q, 2H), 1.43 (d, 3H) ppm.

Calc. for $C_3H_5OS_2Cu$ (%): C 19.5, S 34.7, Cu 34.4; found: C 19.8, S 35.5, Cu 34.2.

2.1.3. Tin (IV) Ethyl Xanthate (SnXan) synthesis

3.5 g of potassium ethyl xanthate was dissolved in 20 ml of de-ionized water and added drop wise to a solution of tin(IV) chloride pentahydrate (1.4 g) dissolved in 20 ml of de-ionized water. This solution was then stirred for 24 hours. The resulting orange paste was then dried at 40 °C, resulting in a dark cream powder. It is worth noting that this precursor is very thermally unstable and will decompose gradually over a period of a week after synthesis.

^{1}H NMR (300 MHz, $CDCl_3$): $\delta = 4.55$ (q, 8H), 1.49 (t, 12H) ppm.

Calc. for $C_{12}H_{20}O_4S_8Sn$ (%): C 23.9, S 42.5, Sn 19.7; found: C 22.7, S 42.3, Sn 20.2.

2.1.4. Zinc Ethyl Xanthate (ZnXan) synthesis

Zinc(II) chloride (0.7 g) was dissolved in 20 ml of de-ionized water, and 3.5 g of potassium ethyl xanthate was dissolved in 20 ml of de-ionized water. Then, the zinc chloride solution was added drop wise to the the potassium xanthate solution, and the resulting solution was stirred for 24 hours. The white precipitate was filtered off, rinsed with de-ionized water, and dried under vacuum at 50 °C revealing a a white powder.

^{1}H NMR (300 MHz, $CDCl_3$): $\delta = 4.59$ (q, 4H), 1.49 (t, 6H) ppm.

Calc. for $C_6H_{10}O_2S_4Zn$ (%): C 23.4, S 41.7, Zn 21.2; found: C 23.6, S 41.5, Zn 21.4.

2.2. Substrate Pre-treatment

Prior to deposition, each substrate was ultra-sonically cleaned in ethanol for 10 minutes. After cleaning, the substrates were dried and an inert gas was blown onto the films to ensure no remaining dirt was trapped.

2.3. CZTS Deposition

Metal xanthates were dissolved into a solution of 5 ml pyridine and 1 ml 1,2-dichlorobenzene. The solution was then stirred for roughly 10 minutes, allowing for the precursors to dissolve. Once dissolved, these solutions were

loaded into the spray coater and deposited onto Indium Tin Oxide (ITO) coated glass for 10 seconds. The spray distance and orientation remained constant for each iteration, a horizontal distance of 10 cm. These samples were then heated to 160 °C for 30 minutes to allow for complete decomposition of the xanthates into their respective metal sulfides. 160 °C was selected as it was shown to be the lowest temperature at which full CuXan decomposition was noted.

2.4. Device Fabrication

After CZTS deposition occurred, CdS was spin coated (using an EZ6 Schwan technology spin coater) onto the active layer in order to create a photovoltaic device. A CdXan precursor was utilised to form the CdS acceptor layer. The precursor was deposited on the CZTS coated substrate and spun for 30 seconds at 1000 rpm. This was then decomposed at 160 °C for 30 minutes. Then, 50 nm of gold was sputtered on the CdS layer to function as an electrode.

2.5. Characterisation techniques

NMR resonance ^{1}HNMR spectra were recorded on a Bruker Ultrashield 300, using $CDCl_3$ solutions at 300 MHz to the singlet of CDCl3 at 7.26 ppm.

Elemental analysis was carried out using Perkin Elmer Series II CHNS/O Analyzer for carbon and sulfur and a Perkin Elmer NexION 300X for copper, tin and zinc.

TGA data was collected on SII 6300 EXSTAR in an air atmosphere between 50-300 °C, increasing by 5 °C/minute.

The thickness of active layer surfaces were characterised in air using Veeco 3100 scanning probe microscope (SPM).

Optical characteristics of the samples were measured at room temperature using a Cary 5000 UV-vis absorption spectrometer at a rate of 400 nm/s, between 350–750 nm. One cycle was taken for each sample.

A Zeiss ΣIGMA Scanning Electron Microscopy (SEM) operating at 5.0 kV was used to determine the morphology, size of the deposited films, while the composition was analysed by Energy Dispersive Spectroscopy (EDS) on an X-Act (Oxford Instrument) coupled with the previously mentioned SEM device.

Crystal structures were determined using X-ray diffraction (XRD). XRD patterns were collected using a D8 Advance diffractometer (Bruker) equipped

with a copper anode (Cu-Kα radiation $\lambda = 0.154$ nm) over the angular range of $10^o < 2\theta < 90^o$ with a step size of 0.01^o at 40 kV and 35 mA.

Current-voltage measurements were made using a CHI600E electrochemical workstation under illumination at AM1.5 G (100 mW cm^{-2}) light intensity.

3. Results and Discussion

3.1. Precursor Characterisation

TGA was initially utilised, with a scanning temperature range of 50-300 °C at a ramping temperature of 5 °C/min, to determine the decomposition behaviour of the metal xanthates into their respective metal sulfides, see **Figure 2**.

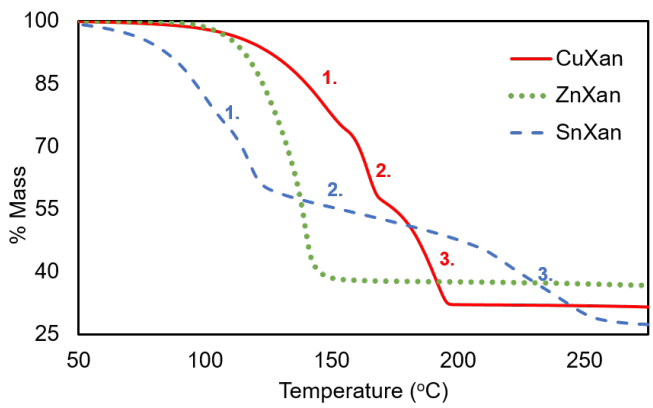

Figure 2: TGA of precursors used in deposition, from 50-300 °C at a ramping temperature of 5 °C/min. Red and blue numbers are shown on the profiles for CuXan and SnXan respectively, to emphasise the three stages of decomposition as shown in **Figure 1**.

All xanthate precursors show the expected decomposition behaviour below 160 °C, however, their initial decomposition temperatures vary, as does the steepness of the decomposition curves (as shown in **Figure 2**). Both CuXan and ZnXan start initial decomposition at roughly 115 °C, though, their decomposition profiles are rather different. ZnXan shows a quite steep one step profile, while CuXan displays a shallower decomposition profile revealing three distinct steps (shown by red numbers on **Figure 2**), coinciding with the elimination stages in the Chuagaev elimination reaction (as numbered in **Figure 1**) [30]. SnXan also shows a similar three step decomposition as CuXan (as shown by blue numbers in **Figure 2**). It can also be seen that

despite SnXan having the lowest thermal stability, the presence of a long, shallow intermediate step suggests a slow rate of decomposition, as steeper gradients relate to faster rates of decomposition.

Despite the variation in decomposition profiles, all xanthates were shown to have observed percentage mass losses that align closely with the theoretical values calculated (see **Table 1**).

Table 1: The experimental mass losses of the used precursors at 300 °C and the theoretical percentage mass loss of the precursors after xanthate decomposition.

Precursor	**Observed Mass Loss**	**Theoretical Mass Loss**
CuXan	31.74 %	31.25 %
ZnXan	36.56 %	31.66 %
SnXan	27.52 %	30.29 %

This correlation shown in **Table 1** suggests the appropriate decomposition pathway to the metal sulfide, providing evidence for these metal xanthates to be viable precursor materials for the deposition of their respective metal sulfides.

3.2. CZTS Thin Film Characterisation

The investigation into the fabrication of CZTS solar cells via xanthate precursors looked into alterations of the xanthate ratios. This can help to determine the effect that the chemical composition had on the active layers and therefore the devices. **Table 2** shows the name used to identify the seven different compositions investigated, as well as the amount of each xanthate used in the precursor mix and their recorded thicknesses from AFM analysis.

These samples were then investigated using SEM/EDS (**Figure 3** and **4**), XRD (**Figure 5** and **6**) and UV-vis (**Figure 7**).

As shown in **Figure 3 a)**, CZT displays a very granular layer, with few crystals evenly blended throughout the material. For all variations from CZT, these crystalline areas are noted to be more prevalent, with CZ2T and CZT2 (shown in **Figure 3 c)** and **e)** respectively) displaying large patches of this crystalline phase. EDS analysis was conducted on these sites to colourise the images depending on the element. Cu is shown in red, Zn in green, and Sn in blue. From this analysis (see **Figure 3 d)** as an example) it

Table 2: Labels and descriptions of the investigated compositions of CZTS devices deposited.

Label	CuXan(g)	ZnXan(g)	SnXan(g)	Thickness
CZT	0.33	0.34	0.22	1.53 μm
C2ZT	0.66	0.34	0.22	1.65 μm
CZ2T	0.33	0.68	0.22	1.62 μm
CZT2	0.33	0.34	0.44	1.69 μm
C0.5ZT	0.165	0.34	0.22	1.48 μm
CZ0.5T	0.33	0.17	0.22	1.43 μm
CZT0.5	0.33	0.34	0.11	1.35 μm

was determined that these crystalline phases displayed a strong green colour, attributing these phases to Zn.

This corresponds with previous observations made in the literature showing that ZnS phases can often form within the CZTS layer [35]. This reduces the stoichiometric accuracy of CZTS within the active layer and increases the length of charge transfer, which in turn reduces exciton generation and increases recombination of excitons. Therefore this ZnS phase can be stated as a detrimental feature of the active layer. This detrimental feature was noted in all devices except CZ0.5T (see **Figure 3 g)**, and **4**), the zinc poor sample, which appears the most crystalline out of the samples.

Figure 4 b) shows that these crystal phases appear to be a blend of Cu-rich and Sn-rich areas, suggesting further detrimental phases to be present within the device. These detrimental phases are likely to be copper sulfide ($Cu_{2\text{-}x}S$) and copper tin sulfide (Cu_2SnS_3), as these have also been previously noted in CZTS active layers [32, 35, 36].

To confirm the presence of these additional phases XRD was conducted on the deposited samples. **Figure 5** shows the XRD diffractogram for CZT, with the position of each phase noted on the pattern. **Figure 6** shows a comparison for samples with varying Cu, Zn and Sn compositions.

In **Figure 5** characteristic kesterite (Cu_2ZnSnS_4) [36], (JSCPDS No. 26-0575) could be seen at roughly 2θ= 18, 23, 28, 33, 44, 47 and 56 °. This shows a good alignment between the material and expected diffractogram, providing evidence of successful deposition. However, it is important to note that other crystal phases are likely to also be present. It has also been

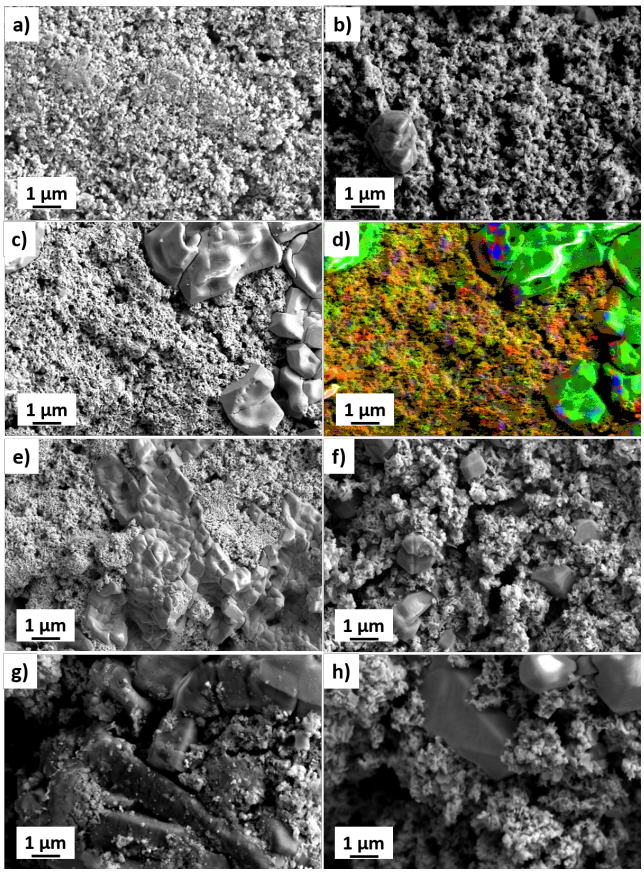

Figure 3: SEM images of a) CZT, b) C2ZT, c) CZ2T, e) CZT2, f) C0.5ZT, g) CZ0.5T and h) CZT0.5. d) shows an EDS mapping image of c) CZ2T, to function as an example for the observed features. For the EDS image Cu is shown in red, Zn in green and Sn in blue.

reported that $Cu_{2-x}S$ (JCPDS No. 47-1748), Cu_2SnS_3 (JCPDS No. 27-0198) and ZnS (JCPDS No. 79-2204) crystal phases have been detected in CZTS thin films [32, 36]. $Cu_{2-x}S$ has expected diffraction peaks at 2θ=23, 26, 30, 32, 37, 39, 43, 45, 48, 51 and 56 °. Cu_2SnS_3 diffraction peaks could be located at roughly 2θ= 16, 18, 21, 24, 28, 31, 34, 38, 42, 48 and 51 °. Diffraction peaks located at 27, 28, 30, 40, 56 and 63° (2θ) could also suggest the presence of ZnS crystal phases within the analysed samples. As the diffraction peaks of these crystal structures often align, the comparison of multiple peaks is vital to determine the variation in crystal phase.

From **Figure 6 a)**, it is apparent that there are two significant variations

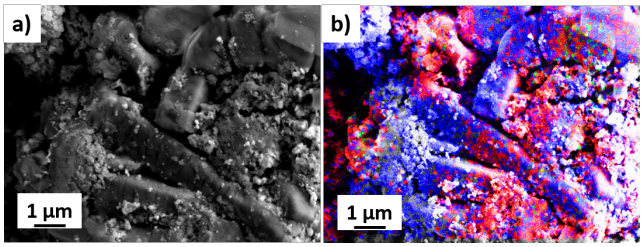

Figure 4: SEM image of a) CZ0.5T. b) shows an EDS mapping image of a) CZ0.5T. For the EDS image Cu is shown in red, Zn in green and Sn in blue.

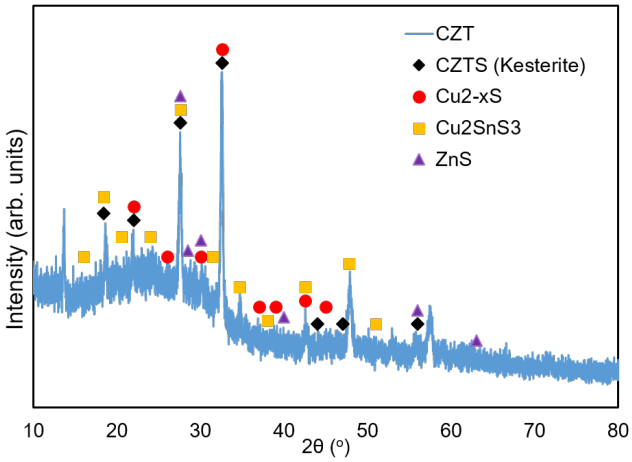

Figure 5: XRD analysis of CZTS using the xanthate mix CZT. All expected peaks for expected phases are shown on the diffractogram.

in the diffractograms when altering the amount of CuXan in the precursor mix. These peaks occur at roughly 2θ= 16 and 21 °, and suggest the presence of Cu_2SnS_3. It can be said that the higher CuXan load within the precursor mix results in increased intensity for these peaks. Therefore, the increase in CuXan within the material causes the additional phase of Cu_2SnS_3 to become more prevalent, which could act as a barrier for carrier transport [36].

Figure 6 b) displays the variation between the diffractograms with altering ZnXan load in the precursor. The presence of two additional phases can be seen with increasing ZnXan load. The increased presence of an additional ZnS phase can be deduced from the increasing intensity of peaks seen at 2θ= 30 and 56 °. More intense peaks at 2θ= 25 and 31 ° suggest an additional layer of Cu_2SnS_3, while the reduced intensity of 2θ= 28 ° could suggest a

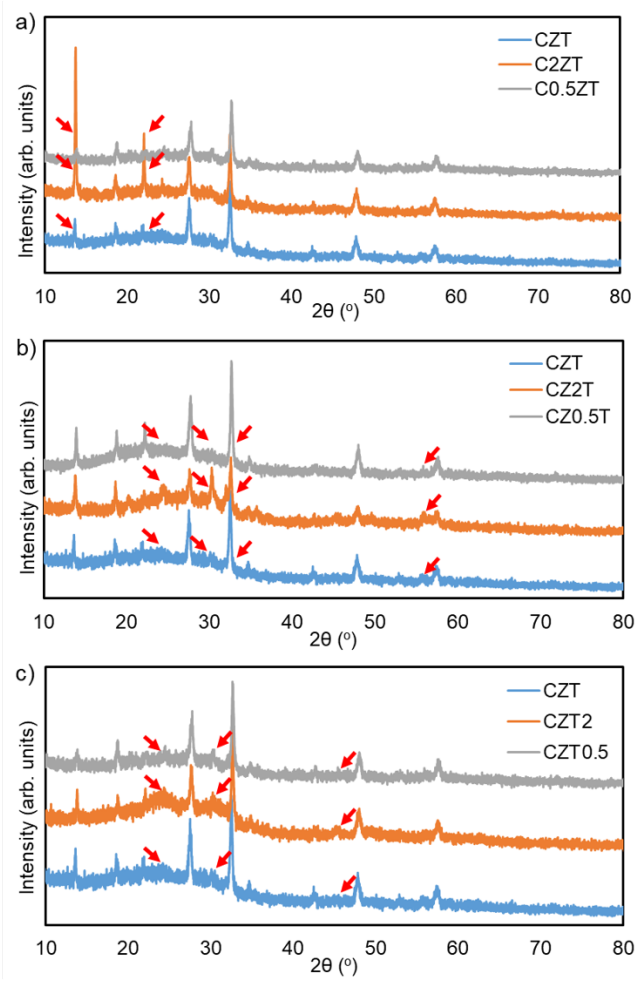

Figure 6: XRD analysis of CZTS xanthate mixes. **a)** presents peaks for CZT, C2ZT and C0.5ZT with key peaks at 2θ= 16 and 21 ° highlighted by red arrows; **b)** reports the peaks for CZT, CZ2T and CZ0.5T with key peaks at 2θ= 25, 30, 31 and 56 ° highlighted by red arrows; and **c)** shows peaks for CZT, CZT2 and CZT0.5 with two bumps noted at 2θ= 25 and 30 ° and a key peak seen at at 2θ= 44 ° highlighted by red arrows.

lower amount of CZTS. It is also worth noting that there is less variation between the intensity of the peaks seen in the diffractogram for CZ2T. This could suggest that the sample is highly polycrystalline, resulting in reduced charge transport and increased recombination of excitons [36, 37]. The low ZnXan load also displays an increase in intensity for 2θ= 31 °, suggesting the presence of Cu_2SnS_3, this is an expected result due to the lower availability

of ZnS to form CZTS.

As seen in **Figure 6 c)**, after the increase in SnXan load the sample appears to become more amorphous, displaying two bumps at 2θ= 25 and 30 °. This suggests the presence of a polycrystalline structure of $Cu_{2-x}S$ with small crystals. An additional small peak can also be seen at 2θ= 44 °, which also correlates to the presence of CZTS, leading to the presumption that the CZT2 layer produces the most stoichiometric sample. For the low SnXan sample it can also be seen that there is a decrease in the peak seen at 2θ= 16 °, this is likely due to the reduced quantity of Cu_2SnS_3 able to be formed.

From the XRD analysis, it can be stated that all variations from CZT either causes the addition of further crystal phases or the reduction of the CZTS crystal phase, lowering the quantity of CZTS and increasing the length of the charge transport route for generated excitons, resulting in less generation and more recombination of excitons. However, the CZT2 sample revealed an additional kerestite peak (as seen in **Figure 6**), which could suggest a higher quality CZTS precursor mix.

To further understand the potential these active layers have as photovoltaic devices, optical investigations into the chemical compositions were undertaken. Absorbance spectra were collected for each sample, to study the optical properties of the active layers (see **Figure 7**).

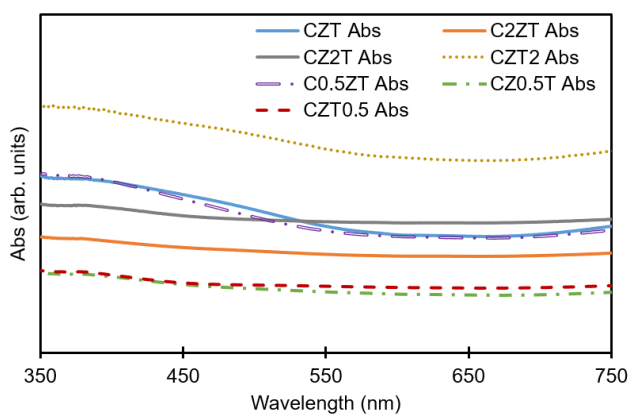

Figure 7: UV-vis absorbance spectra of deposited CZTS active layer

The first key observation seen in **Figure 7** relates to the varying intensity in absorbance between the active layers. While it can be stated that the absorbance intensity is affected by the thickness (see **Table 2**) of the active layer, as the thickest layer (CZT2) has the highest absorbance and the

two thinnest layers (CZ0.5T and CZT0.5) have the lowest absorbance, this does not fit as a description for all profiles. While it can be said that the thickest layer is the most absorbing, it is only 0.04 μm thicker than the C2ZT layer, which is the third least absorbing layer. Furthermore, the difference in thickness between C0.5ZT and CZT is 0.05 μm (a similar difference seen between C2ZT and CZT2), yet their absorbance profiles appear at a similar level across the spectra. Therefore, secondary phases that appear in the active layers are likely to have a more significant effect on their absorbance profiles.

It can be seen from **Figure 7** that only three samples (CZT, CZT2 and C0.5ZT) show significant change in absorbance across the spectra, increasing in absorbance between 350-550 nm. From the XRD analysis (**Figure 6a)** and **6c)**) it can be stated that these three samples have fewer additional crystal phases, with a crystal structure that more closely resembles that of CZTS. Furthermore, visually these three samples (CZT, CZT2 and C0.5ZT) look similar, as confirmed by SEM images (**Figure 3 a), e) and f)**).

It is suggested that the observed UV-vis absorbance profile is due to the increased presence of the CZTS crystal phase, as the spectra match previously obtained spectra of CZTS [32]. Tauc plots were then generated to calculate the band gap of each active layer, extrapolating the band gaps from the straight lines seen in **Figure 8**.

The value of the band gaps calculated for CZT, C2ZT and CZ2T all fit within the same region of roughly 1.93 eV, while CZT2 exhibits the lowest value of 1.73 eV (see **Figure 8 a)**). This has previously been attributed to the fewer impurities within the active layers, especially the formation of $Cu_{2-x}S$ [17, 32]. This would also mean that the two bumps, seen at at 2θ= 25 and 30 ^{o} on the CZT2 diffraction pattern (**Figure 6 c)**) can also be attributed to CZTS kesterite peaks that appear in similar areas.

Figure 8 b) shows that the band gap becomes larger as precursor loads are reduced. As discussed for **Figure 8 a)**, these increases in band gap energy could be attributed to the presence of extra phases and contaminants, such as $Cu_{2-x}S$, Cu_2SnS_3 and ZnS.

From this analysis, it can be assumed that a stoichiometric mixture of xanthate precursors does not result in a stoichiometric product. Instead, additional SnXan is required to yield results similar to that expected for CZTS. Therefore, it can be deduced that the composition of these films will still be affected by the rate in which these components decompose.

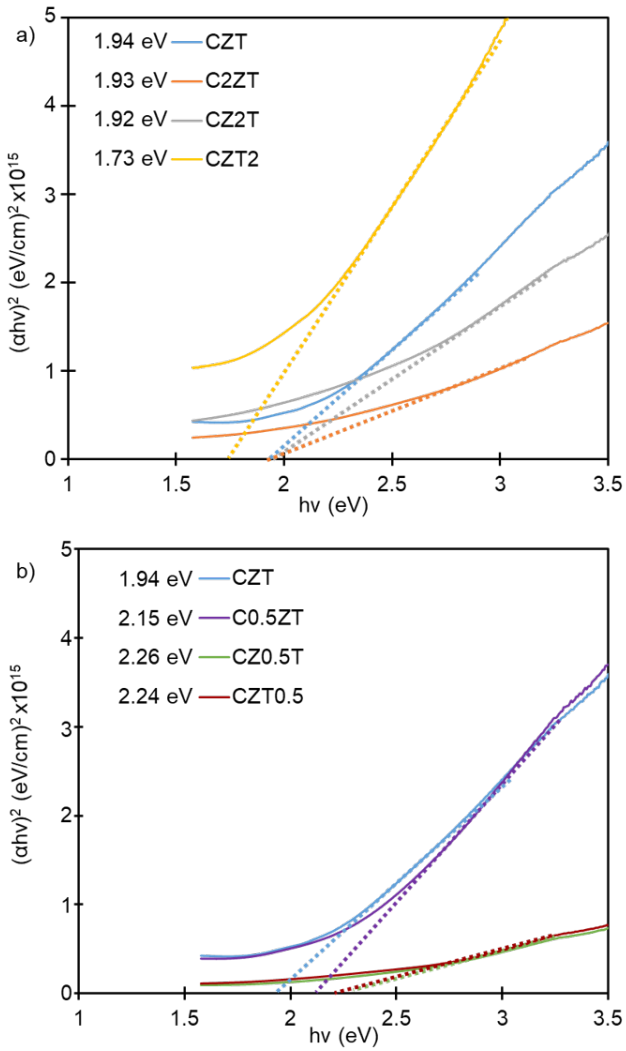

Figure 8: Tauc plots of **a)** increased metal load for CZTS solar cells and **b)** decreased metal load for CZTS solar cells. Band gap values are given in the legend.

3.3. Kinectic analysis of decomposition

In order to work out the rate constants for the decomposition for each of these precursors, and therefore make a comparison based from this kinetic component, isothermal TGA measurements were taken at 160 °C (the deposition temperature used in the previous depositions) for each precursor.

The first step towards making these calculations is to plot a graph of β

against time. β is dependant on weight loss and is calculated by:

$$\beta = \frac{wi - wt}{wi - wf} \tag{1}$$

where wi is the initial weight, wt the weight at each time and wf the final weight.

These isothermal scans then require additional analysis to yield insight into the mechanism of thermal degradation. It is generally seen that materials follow [38]:

$$\frac{\delta\beta}{\delta t} = k(T)(1-\beta)^n \tag{2}$$

where t is time, k(T) the kinetic rate constant at the analysed temperature and n the order of reaction.

It is important to note that this rate term is temperature dependant and is expressed by $k(T)$ [39]. In order to extract useful data from the graph it needs to be linearised, to achieve this the kinetic standard method was used, using the following equation [38]:

$$ln\frac{\delta\beta}{\delta t} = ln[k(T)] + nln(1-\beta) \tag{3}$$

A plot of $\ln(\delta\beta/\delta t)$ vs $ln(1-\beta)$ results in a gradient of n (giving the units for k) and an intercept that allows for the calculation of k. This is shown graphically in **Figure 9**.

Following this approach it was shown that the rate constants of CuXan and ZnXan align very well, at 1.26 and 1.24 s^{-1} respectively. This would suggest that the rates at which these two xanthates decompose are very similar, with ZnXan decomposing faster. This mirrors results from **Figure 2**, showing similar initial decomposition temperatures and ZnXan showing a steeper decomposition curve. However, the rate constant for SnXan differs significantly. Despite having the lowest initial decomposition temperature, it has the smallest rate constant (1.09 s^{-1}) suggesting the slowest reaction. This is reflected in the decomposition profile of SnXan, by the long, gradual intermediate decomposition peak. Therefore, it was noted that additional SnXan is required due to the small rate constant of decomposition. As the other two xanthates decompose faster, more SnXan would need to be added to allow for the correct chemical composition. However, this is not an effective

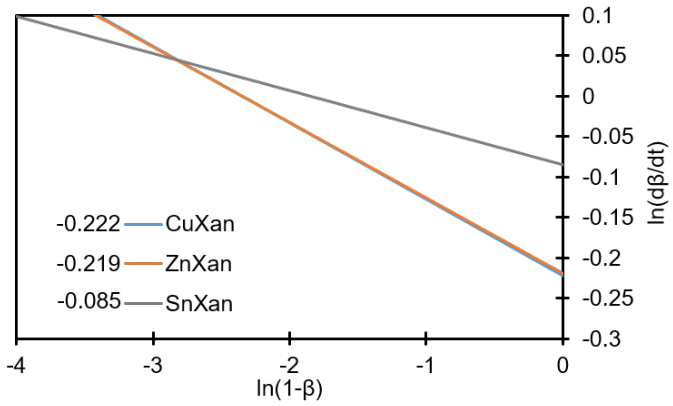

Figure 9: A plot of $\ln(\delta\beta/\delta t)$ vs $ln(1-\beta)$. The intercept values are written in the legend and allow for the calculation of k. In this figure CuXan and ZnXan appear almost identically, masking the appearance of CuXan

solution and to better address this problem one, or a combination, of three key ways could be implemented:

1. As the rate constant is temperature dependent, an investigation into how the rate constants vary with temperature could help to align them.
2. The decomposition of these metal xanthates is initiated by a syn-elimination, of a beta-hydrogen, via a 6-membered cyclic transition state to form an alkene (as shown in **Figure 1**) [30]. Therefore, increasing the number of beta-hydrogens on the 'R' group of the metal xanthate precursors would increase the rate of the reaction. Implementing this for SnXan could align the rate constants of the xanthate precursors. However, SnXan is already very thermally unstable and this would potentially further reduce the thermal stability, making the precursor difficult to effectively implement.
3. Using the same idea as point 2, the amount of beta-hydrogens for CuXan and ZnXan could be reduced, thereby allowing the reactions to be slowed down and match that of SnXan. However, this would increase the thermal stability of the precursors and might result in the need for higher temperatures for decomposition.

From these descriptions, it is assumed that CZT2 produces the most pure CZTS layers, and is hypothesised to function as the most effective photovoltaic solar cell.

3.4. Photovoltaic device performance

To determine how these materials function as photovoltaic devices, current-voltage (I–V) curves (shown in **Figure 10**) were collected from the prepared samples, to establish the influence of the abovementioned chemical and optical differences on key photovoltaic parameters.

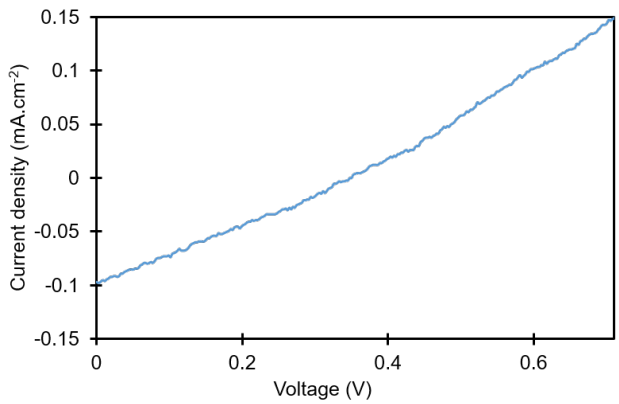

Figure 10: Current-voltage curves of CZT2 under illumination with an intensity of 100 mW.cm^{-2}.

It was noted that only one precursor mixture (CZT2) resulted in a functional photovoltaic device (as shown in **Figure 10**). CZT2 had an open circuit potential (Voc) of 0.347 V, similar to that previously reported for a non-stoichiometric CZTS device [7]. The short circuit current (Jsc) and Fill Factor (FF) were calculated to be 1.55 mA.cm^{-2}, and 0.27 respectively, resulting in a PCE efficiency of 0.15 %. It is important to note Voc, Jsc and PCE outperform the previously reported CZTS photovoltaic devices made from metal xanthate precursors (with a Voc of 0.2 V, a Jsc of 1.3 mA.cm^{-2}, and a PCE of 0.11 %), although the FF is reduced from 0.37 to 0.27 [3].

Despite performing well, compared to previously reported CZTS photovoltaic devices deposited using metal xanthate precursors, the PCE is quite low compared to other CZTS photovoltaic devices [4, 6]. This can be attributed to the product of low Jsc and FF values. The lower Jsc can be ascribed to the influence of resistance between different components of the device. This could potentially be dramatically improved through various methods, such as energy level optimisation via introducing layers to enhance carrier mobility and current collection or altering the chemistry and crystal

of current layers through the introduction of additional dopants or post-treatments [7, 40–42]. The low FF value is likely due to high recombination within the device. As recombination occurs at grain boundaries [37], the polycrystalline bumps (at 2θ= 25 and 30 ^{o} in **Figure 6 c)**) would suggest smaller crystal sizes and therefore more recombination sites, leading to a lower FF. It is possible to improve this by increasing the decomposition temperature used, or adding an additional annealing step, as this has previously been shown to increase crystallinity [3, 43].

Furthermore, it is important to point out that the performance of typical CZTS devices are also limited by a Voc deficit, dominated by heterojunction interface recombination [15]. Therefore, it is important to further optimise the design of these devices and reduce detrimental secondary phases.

4. Conclusions

This investigation looked into the use of metal xanthate precursors in the deposition of CZTS thin films via spray coating, helping to promote this manufacturing route for possible future commercial viability.

SEM-EDS analysis of zinc rich and copper poor precursor mixtures showed significant areas of ZnS crystalisation, a detrimental feature for the devices as it reduces the quantity of CZTS and increases the length of the charge transport route for generated excitons, resulting in less generation and more recombination of excitons. XRD analysis confirmed these findings and further showed the presence of $Cu_{2-x}S$, Cu_2SnS_3, and ZnS contaminating phases in almost all thin films. The tin rich sample (CZT2) was shown to contain the least contamination and therefore, the most accurate overlap with the CZTS crystal structure. A tin rich precursor mixture was required due to the slower decomposition of SnXan compared to that of CuXan and ZnXan, reflected in the rate constants for decomposition as 1.09, 1.26 and 1.24 s^{-1} respectively. Thus requiring more SnXan to be added to form the required stoichiometry. This finding was confirmed through UV-vis analysis and the derived Tauc plots, showing that CZT2 had a band gap closer to the expected band gap of 1.5 eV. Photovoltaic devices were made from all CZTS samples described in **Table 2**, with only CZT2 showing significant photoactivity. The produced device displayed an improved Power Conversion Efficiency for a CZTS based metal xanthate deposited photovoltaic device, with a Power Conversion Efficiency of 0.15 %. These findings provide evidence for the need

of further developing this under investigated deposition pathway to develop devices with comparable efficiency and reduced toxicity.

5. Acknowldgements

This work is supported by Natural Science Foundation of China with a project code 51804172; Ningbo Science and Technology Innovation 2025 Key Project (2018B10029); and the International Doctoral Innovation Centre, Ningbo Education Bureau, Ningbo Science and Technology Bureau and the University of Nottingham. The authors would also like to thank Julian Zhu and Kate Yuan for aid in operation of the Bruker D8 Advance diffractometer (XRD) and SII 6300 EXSTAR (TGA), respectively.

References

[1] M. Al-Shakban, P. D. Matthews, N. Savjani, X. L. Zhong, Y. K. Wang, M. Missous, P. O'Brien, The synthesis and characterization of cu2znsns4 thin films from melt reactions using xanthate precursors, Journal of Materials Science 52 (21) (2017) 12761–12771. doi:10.1007/s10853-017-1367-0.

[2] F. Ballipinar, A. C. Rastogi, Tin sulfide (sns) semiconductor photoabsorber thin films for solar cells by vapor phase sulfurization of sn metallic layers using organic sulfur source, Journal of Alloys and Compounds 728 (2017) 179–188. doi:10.1016/j.jallcom.2017.08.295.

[3] A. Fischereder, A. Schenk, T. Rath, W. Haas, S. Delbos, C. Gougaud, N. Naghavi, A. Pateter, R. Saf, D. Schenk, M. Edler, K. Bohnemann, A. Reichmann, B. Chernev, F. Hofer, G. Trimmel, Solution-processed copper zinc tin sulfide thin films from metal xanthate precursors, Monatshefte Fur Chemie 144 (3) (2013) 273–283. doi:10.1007/s00706-012-0882-6.

[4] H. Katagiri, Cu2znsns4 thin film solar cells, Thin Solid Films 480 (2005) 426–432. doi:10.1016/j.tsf.2004.11.024.

[5] C. Q. Liu, B. Wen, X. N. Zhai, T. T. Lun, M. S. Song, N. Wang, S. M. Liu, H. L. Wang, W. W. Jiang, W. Y. Ding, S. C. Xu, W. P. Chai, Cu2znsns4 films with different preferred orientations prepared by pulsed

dc magnetron sputtering from a quaternary ceramic target, Materials Letters 213 (2018) 241–244. doi:10.1016/j.matlet.2017.11.056.

[6] X. B. Song, X. Ji, M. Li, W. D. Lin, X. Luo, H. Zhang, A review on development prospect of czts based thin film solar cells, International Journal of Photoenergydoi:10.1155/2014/613173.

[7] O. Vigil-Galan, M. Espindola-Rodriguez, M. Courel, X. Fontane, D. Sylla, V. Izquierdo-Roca, A. Fairbrother, E. Saucedo, A. Perez-Rodriguez, Secondary phases dependence on composition ratio in sprayed cu2znsns4 thin films and its impact on the high power conversion efficiency, Solar Energy Materials and Solar Cells 117 (2013) 246–250. doi:10.1016/j.solmat.2013.06.008.

[8] S. Ahmed, K. B. Reuter, O. Gunawan, L. Guo, L. T. Romankiw, H. Deligianni, A high efficiency electrodeposited cu2znsns4 solar cell, Advanced Energy Materials 2 (2) (2012) 253–259. doi:10.1002/aenm.201100526.

[9] S. S. Mali, P. S. Shinde, C. A. Betty, P. N. Bhosale, Y. W. Oh, P. S. Patil, Synthesis and characterization of cu2znsns4 thin films by silar method, Journal of Physics and Chemistry of Solids 73 (6) (2012) 735–740. doi:10.1016/j.jpcs.2012.01.008.

[10] A. K. Singh, A. Shrivastava, M. Neergat, K. R. Balasubramaniam, Phase evolution during the electrodeposition of cu-sn-zn metal precursor layers and its role on the cu2s impurity phase formation in cu2znsns4 thin films, Solar Energy 155 (2017) 627–636. doi:10.1016/j.solener.2017.06.063.

[11] T. P. Dhakal, D. N. Ramesh, R. R. Tobias, C. Y. Peng, C. R. Westgate, Ieee, Enhancement of efficiency in cu2znsns4 (czts) solar cells grown by sputtering, in: 39th IEEE Photovoltaic Specialists Conference (PVSC), IEEE Photovoltaic Specialists Conference, Ieee, NEW YORK, 2013, pp. 1949–1952.

[12] P. A. Fernandes, P. M. P. Salome, A. F. da Cunha, Growth and raman scattering characterization of cu2znsns4 thin films, Thin Solid Films 517 (7) (2009) 2519–2523. doi:10.1016/j.tsf.2008.11.031.

[13] Y. Zhu, Y. Q. Chen, T. Shen, J. H. Yi, G. Y. Gan, Q. Huang, Direct current magnetron sputtered cu2znsns4 thin films using a ceramic qua-

ternary target, Journal of Alloys and Compounds 727 (2017) 1115–1125. doi:10.1016/j.jallcom.2017.08.226.

[14] S. Marchionna, P. Garattini, A. Le Donne, M. Acciarri, S. Tombolato, S. Binetti, Cu2znsns4 solar cells grown by sulphurisation of sputtered metal precursors, Thin Solid Films 542 (2013) 114–118.

[15] A. Pu, F. Ma, C. Yan, J. Huang, K. Sun, M. Green, X. Hao, Sentaurus modelling of 6.9% cu2znsns4 device based on comprehensive electrical & optical characterization, Solar Energy Materials and Solar Cells 160 (2017) 372–381.

[16] M. Colina, E. Bailo, B. Medina-Rodriguez, R. Kondrotas, Y. Sanchez-Gonzalez, D. Sylla, M. Placidi, M. Blanes, F. Ramos, A. Cirera, A. P. Rodriguez, E. Saucedo, Optimization of ink-jet printed precursors for cu2znsn(s, se)(4) solar cells, Journal of Alloys and Compounds 735 (2018) 2462–2470. doi:10.1016/j.jallcom.2017.12.035.

[17] S. Kermadi, S. Sali, F. A. Ameur, L. Zougar, M. Boumaour, A. Toumiat, N. N. Melnik, D. W. Hewak, A. Duta, Effect of copper content and sulfurization process on optical, structural and electrical properties of ultrasonic spray pyrolysed cu2znsns4 thin films, Materials Chemistry and Physics 169 (2016) 96–104. doi:10.1016/j.matchemphys.2015.11.035.

[18] S. Kermadi, S. Sali, L. Zougar, M. Boumaour, R. Gunder, S. Schorr, V. Izquierdo-Roca, A. Perez-Rodriguez, An in-depth investigation on the grain growth and the formation of secondary phases of ultrasonic-sprayed cu2znsns4 based thin films assisted by na crystallization catalyst, Solar Energy 176 (2018) 277–286. doi:10.1016/j.solener.2018.10.045.

[19] M. Mokhtarimehr, I. Forbes, N. Pearsall, Environmental assessment of vacuum and non-vacuum techniques for the fabrication of cu2znsns4 thin film photovoltaic cells, Japanese Journal of Applied Physics 57 (8S3) (2018) 08RC14.

[20] T. Ozdal, H. Kavak, Comprehensive analysis of spin coated copper zinc tin sulfide thin film absorbers, Journal of Alloys and Compounds 725 (2017) 644–651. doi:10.1016/j.jallcom.2017.07.209.

[21] M. Bishop, B. Akinwolemiwa, L. Zhang, C. Peng, D. Hu, Morphological, optical and electrical properties of spray coated zinc ethyl xanthates for decomposition within a poly (3-hexylthiophene-2, 5-diyl) matrix, in: E3S Web of Conferences, Vol. 80, EDP Sciences, 2019, p. 03012.

[22] Z. Wang, R. Gauvin, G. P. Demopoulos, Nanostructural and photo-electrochemical properties of solution spin-coated cu2znsns4-tio2 nanorod forest films with an improved photovoltaic performance, Nanoscale 9 (22) (2017) 7650–7665. doi:10.1039/c7nr01422h.

[23] A. Weber, R. Mainz, H. Schock, On the sn loss from thin films of the material system cu–zn–sn–s in high vacuum, Journal of Applied Physics 107 (1) (2010) 013516.

[24] A. Weber, H. Krauth, S. Perlt, B. Schubert, I. Kötschau, S. Schorr, H. Schock, Multi-stage evaporation of cu2znsns4 thin films, Thin Solid Films 517 (7) (2009) 2524–2526.

[25] M. T. Bishop, M. Tomatis, W. Zhang, C. Peng, G. Z. Chen, J. He, D. Hu, Assessment of toxicity reduction in zns substituted cds:p3ht bulk heterojunction solar cells fabricated using a single-source precursor deposition, Sustainable Energy & Fuels (2019) 1–8.doi:10.1039/c9se00123a.

[26] M. A. Buckingham, A. L. Catherall, M. S. Hill, A. L. Johnson, J. D. Parish, Aerosol-assisted chemical vapor deposition of cds from xanthate single source precursors, Crystal Growth & Design 17 (2) (2017) 907–912. doi:10.1021/acs.cgd.6b01795.

[27] A. L. Johnson, M. S. Hill, G. Kociok-Kohn, K. C. Molloy, A. L. Sudlow, The first crystallographically-characterised cu(ii) xanthate, Inorganic Chemistry Communications 49 (2014) 8–11. doi:10.1016/j.inoche.2014.09.003.

[28] G. Kociok-Kohn, K. C. Molloy, A. L. Sudlow, Molecular routes to cu2znsns4: A comparison of approaches to bulk and thin-film materials, Canadian Journal of Chemistry 92 (6) (2014) 514–524. doi:10.1139/cjc-2013-0497.

[29] S. Palaty, P. V. Devi, K. J. Mary, Characterisation and thermal decomposition behaviour of xanthate compounds, Progress in Rubber Plastics and Recycling Technology 26 (4) (2010) 199–213.

[30] E. Velez, J. Quijano, R. Notario, J. Murillo, J. F. Ramirez, Computational study of the mechanism of thermal decomposition of xanthates in the gas phase (the chugaev reaction), Journal of Physical Organic Chemistry 21 (9) (2008) 797–807. doi:10.1002/poc.1383.

[31] Y. B. K. Kumar, G. S. Babu, P. U. Bhaskar, V. S. Raja, Preparation and characterization of spray-deposited cu(2)znsns(4) thin films, Solar Energy Materials and Solar Cells 93 (8) (2009) 1230–1237. doi:10.1016/j.solmat.2009.01.011.

[32] M. Sampath, K. Sankarasubramanian, J. Archana, Y. Hayakawa, K. Ramamurthi, K. Sethuraman, Structural, optical and photocatalytic properties of spray deposited cu2znsns4 thin films with various s/(cu plus zn plus sn) ratio, Materials Science in Semiconductor Processing 87 (2018) 54–64. doi:10.1016/j.mssp.2018.07.001.

[33] V. Agrawal, K. Jain, L. Arora, S. Chand, Synthesis of cds nanocrystals in poly(3-hexylthiophene) polymer matrix: optical and structural studies, Journal of Nanoparticle Research 15 (6) (2013) 1–14. doi:10.1007/s11051-013-1697-z.

[34] N. Yordanov, V. Gancheva, B. Mladenova, G. Grampp, Kinetic studies on the reaction between copper (ii) ions and some dithiocarbonates using stopped-flow technique, Inorganic chemistry communications 6 (1) (2003) 54–57.

[35] M. Espindola-Rodriguez, M. Placidi, O. Vigil-Galan, V. Izquierdo-Roca, X. Fontane, A. Fairbrother, D. Sylla, E. Saucedo, A. Perez-Rodriguez, Compositional optimization of photovoltaic grade cu2znsns4 films grown by pneumatic spray pyrolysis, Thin Solid Films 535 (2013) 67–72. doi:10.1016/j.tsf.2012.12.082.

[36] N. Kattan, B. Hou, D. J. Fermin, D. Cherns, Crystal structure and defects visualization of cu2znsns4 nanoparticles employing transmission electron microscopy and electron diffraction, Applied Materials Today 1 (1) (2015) 52–59. doi:10.1016/j.apmt.2015.08.004.

[37] S. Aslam, F. Mustafa, M. A. Ahmad, M. Saleem, M. Idrees, A. S. Bhatti, Photovoltaic performance and impedance spectroscopy of zns-cu-go nanocomposites, Ceramics International 44 (1) (2018) 402–408. doi:10.1016/j.ceramint.2017.09.191.

[38] J. Vega-Baudrit, M. Sibaja-Ballestero, P. Vazquez, S. Nunez, J. M. Martin-Martinez, L. Benavides-Rodriguez, Kinetics of isothermal degradation studies in adhesives by thermogravimetric data: Effect of hydrophilic nanosilica fillers on the thermal properties of thermoplastic polyurethane-silica nanocomposites, Recent Patents on Nanotechnology 2 (3) (2008) 220–226. doi:10.2174/187221008786369679.

[39] Y. Shen, D. R. Nagaraj, R. Farinato, P. Somasundaran, Study of xanthate decomposition in aqueous solutions, Minerals Engineering 93 (2016) 10–15. doi:10.1016/j.mineng.2016.04.004.

[40] R. Kroon, M. Lenes, J. C. Hummelen, P. W. M. Blom, B. De Boer, Small bandgap polymers for organic solar cells (polymer material development in the last 5 years), Polymer Reviews 48 (3) (2008) 531–582. doi:10.1080/15583720802231833.

[41] Y. S. Kwon, J. Lim, H. J. Yun, Y. H. Kim, T. Park, A diketopyrrolopyrrole-containing hole transporting conjugated polymer for use in efficient stable organic-inorganic hybrid solar cells based on a perovskite, Energy & Environmental Science 7 (4) (2014) 1454–1460. doi:10.1039/c3ee44174a.

[42] S. Rondiya, A. Rokade, P. Sharma, M. Chaudhary, A. Funde, Y. Jadhav, S. Haram, H. Pathan, S. Jadkar, Czts/cds: interface properties and band alignment study towards photovoltaic applications, Journal of Materials Science-Materials in Electronics 29 (5) (2018) 4201–4210. doi:10.1007/s10854-017-8365-5.

[43] R. A. Joshi, M. Gupta, D. Phase, Annealing induced modifications in physicochemical and optoelectronic properties of cds/cuingase2 thin film, Solar Energy 177 (2019) 1–7.